Kinetics of Atomic Nitrogen Photofragment Produced by Laser Photodissociation of N_2O

Steven F. Adams* and Charles A. DeJoseph, Jr.

Air Force Research Laboratory, Wright Patterson Air Force Base, Ohio 45433

Christopher C. Carter and Terry A. Miller

Laser Spectroscopy Facility, Department of Chemistry, The Ohio State University, Columbus, Ohio 43210

James M. Williamson

Innovative Scientific Solutions Inc., Dayton, Ohio 45440

Received: October 23, 2000; In Final Form: March 15, 2001

The kinetics of ground-state atomic nitrogen photofragments produced by laser photodissociation of nitrous oxide have been investigated using two-photon LIF. A single 207 nm laser pulse was used for both N_2O photolysis and N atom two-photon LIF. The dependency of the LIF signal with laser power indicated that the observed N atom fragment was produced by N_2O dissociation via single-photon absorption. Effects of translational energy of the N atom fragment were detected in collisional quenching rates of the two-photon excited N atom $(3p)^4S$ state as observed in the decay lifetime of the induced fluorescence. The mean translational kinetic energy of the N atom fragment was determined to be 0.6 ± 0.2 eV from the quenching data. An analysis of the Doppler broadened absorption line shape of the recoiling atomic nitrogen confirmed the mean kinetic energy and further presented a model speed distribution and anisotropy parameter that was consistent with the line shape data. The NO translational and internal energies of 0.3 ± 0.1 eV and 0.2 ± 0.1 eV, respectively, were also assigned by momentum and energy conservation.

Introduction

Atomic nitrogen is commonly produced for laboratory or industrial applications by dissociation of N_2 in a glow discharge. A glow discharge source is a relatively efficient method of N atom production, but the various radical species produced in the discharge source as well as the excessive background radiation can be prohibitive for some laboratory measurements. Laser photolysis of a nitrogen containing molecule can also be considered for atomic nitrogen production, with the advantage of eliminating the radical species and background radiation concerns of a discharge source. The photolysis technique would be especially useful if a molecule is used with a dissociation energy that matches the photon energy for the N atom two-photon absorption laser-induced fluorescence (TALIF) detection technique. The molecule can thereby be photodissociated and the atomic photofragment detected by TALIF within the same laser pulse. Both H atoms and O atoms have previously been produced and probed by TALIF in this manner. The H and O atoms were produced from the photolysis of C_2H_2[1] and NO_2[2] with laser wavelengths of 205 and 226 nm, respectively, and probed by TALIF with the same laser pulse. Such photodissociation/TALIF techniques have been used to calibrate the TALIF signal collection view factor in a reactor cell that has spatial regions of restricted view. The reactor cell can be uniformly filled with the precursor molecule, which results in a spatially uniform atomic density and corresponding TALIF intensity, except where the view is restricted. The data from a spatial scan of the photodissociation induced TALIF signal in a reactor cell can be used to determine the cell view factor for use with other atomic sources, such as a discharge.

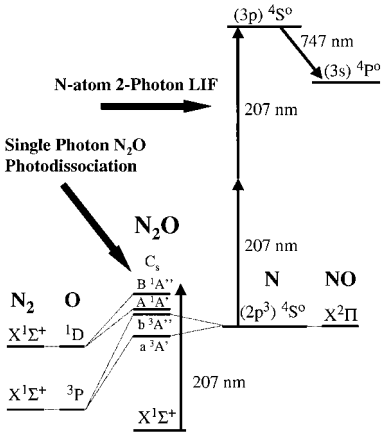

Figure 1. Energy level diagram of N_2O, including dissociative pathways from N_2O excited states obtainable by absorption of 207 nm radiation with resulting N_2-O and N−NO photofragment pairs shown along with a superposition of the N atom TALIF process.

Nitrous oxide is investigated here as a suitable precursor for producing ground-state N atoms by photodissociation with subsequent TALIF via the $(3p)\ ^4S^o_{3/2}$ state using 207 nm laser light. An energy level diagram for N_2O is presented in Figure 1 and shows the dissociative pathways from N_2O excited states below 6 eV,[3] which is the photon energy of 207 nm radiation. The resulting photofragment pairs of N_2-O and N−NO are both included in Figure 1, along with a superposition of the N atom energy levels involved in the subsequent TALIF process.

* Corresponding author.

10.1021/jp0039058 CCC: $20.00
Published on Web 06/05/2001

Since the photodissociation channel resulting in N_2 and $O(^1D)$ involves spin-allowed transitions, this combination of photofragments is the predominate photolysis pathway compared to the path producing NO and $N(^4S)$, which involves spin forbidden transitions. The kinetics of the predominate N_2-O photofragment pair have been studied extensively,[4−7] while no detailed investigation of the NO−N photofragment kinetics has been reported. Suzuki et al.[4] reported laser photodissociation of N_2O at 205 nm, where the percent branching ratios of the primary paths were measured to be

$$\begin{aligned} N_2O \xrightarrow{h\nu} N_2(X^1\Sigma) + O(^1D) \qquad (\sim 90\%) \\ N_2O \xrightarrow{h\nu} N_2(X^1\Sigma) + O(^1S) \qquad (\sim 5\%) \\ N_2O \xrightarrow{h\nu} N_2(X^1\Sigma) + O(^3P) \qquad (\sim 2\%) \end{aligned} \tag{1}$$

The secondary dissociative branch that produces the NO−N photofragment pair is

$$N_2O \xrightarrow{h\nu} NO(X^2\Pi) + N(^4S) \tag{2}$$

which has been shown to exist[4,8] but with an upper bound of 2% of the primary process.

Despite the seemingly low yield of N atoms, the photolysis of N_2O is a more efficient source of atomic nitrogen than the photolysis of NO_2 or NO with $\lambda > 200$ nm.[8] Bengtsson and co-workers reported N_2O photolysis and two-photon absorption[9] as the first step in a process that further excited the N atoms from the (3p) $^4S^\circ_{3/2}$ state to a series of Rydberg states by single-photon absorption using a secondary dye laser beam. They produced ground state N atoms in a few hundred milliTorr of N_2O and detected N atoms via TALIF. However, the published data indicated that the upper (3p) $^4S^\circ_{3/2}$ state of the TALIF scheme was severely quenched as the N_2O pressure neared 0.5 Torr. The authors claimed that a lack of a well-defined collision partner in the interaction region prevented any analysis of the quenching. The quenching rate was not stated but, by inspection, can be seen to be much greater than the quenching rate due to N_2 measured at 300 K.[10] This severe quenching could limit the usefulness of the technique, since a higher pressure nitrous oxide environment would be necessary to produce more N atoms. Bengtsson also did not investigate the energetics of the N_2O photodissociation process that produced the N atom fragment, which left in question whether the dissociation was prompted via single- or multiphoton absorption.

In this work, nitrous oxide photodissociation and atomic nitrogen TALIF detection were both accomplished with a single pulse of 207 nm laser radiation. The N_2O photodissociation event that produced the observed N atom fragments was experimentally determined to be a single-photon process. The quenching rate of the N atom (3p) $^4S^\circ_{3/2}$ TALIF upper state was experimentally determined within the laser photolysis region. The N atom (3p) $^4S^\circ_{3/2}$ state quenching by N_2O was then independently investigated using a microwave discharge N atom source and mixing N_2O in the flowing afterglow region. Quenching of the N atom (3p) $^4S^\circ_{3/2}$ state in the photolysis environment was found to have a much higher rate than the N atom (3p) $^4S^\circ_{3/2}$ quenching by N_2O alone in the flowing afterglow, which was attributed to the excessive kinetic energy imparted to the atomic nitrogen photofragment during N_2O photodissociation. The Doppler broadened two-photon absorption line shape of the recoiling atomic nitrogen photofragment was fit with a model kinetic energy distribution of atomic nitrogen. The Doppler analysis provided results consistent with the quenching analysis.

Experiment

A. Two-Photon LIF Detection of Atomic Nitrogen. A single ultraviolet laser pulse was used to both photodissociate N_2O and detect atomic nitrogen by the TALIF technique. Laser excitation for the photodissociation and TALIF technique was at 207 nm with the fluorescence detected at 747 nm.[10] The energy level diagram of the N atom TALIF scheme is included in Figure 1, with the upper state of the scheme being the (3p) $^4S^\circ_{3/2}$ state. For convenience, two different laser configurations were used in separate experiments to generate the 207 nm laser pulse. A Nd:YAG pumped dye laser system including two nonlinear optic crystal frequency conversions was used for the collisional quenching and laser power dependency analyses. The second harmonic output of the Nd:YAG pumped DCM dye to produce a 620 nm beam, which was then frequency doubled with a KDP crystal to generate 310 nm radiation. The doubled dye was then mixed with the residual dye fundamental in a BBO crystal to produce 0.2 mJ of 207 nm radiation. The temporal profile of the 207 nm laser pulse, which was needed for the TALIF quenching analysis, was determined with a photodiode to be roughly Gaussian with a width of 6.0 ns (fwhm). A high-energy ultraviolet variable attenuator was used for the laser power dependency analysis, with the laser pulse energy determined with a pyroelectric joulemeter. A second dye laser, operating with Fluoroscene 2 dye and pumped by a XeCl excimer laser, was employed for the Doppler broadening measurements. The 414 nm dye laser output was frequency-doubled with a BBO to generate 0.2 mJ of 207 nm laser pulse. In both configurations, the atomic nitrogen fluorescence from the 207 nm laser pulse was collected with a single 7.5 cm focal length f/1 lens. The fluorescence was passed through a 10 nm bandwidth interference filter centered at 747 nm and imaged onto a Hamamatsu R928 photomultiplier tube. The temporal response function of the detection system was found to have a time constant of 6.4 ns, which was used in the TALIF quenching analysis. The time-resolved TALIF signal was recorded with a digitizing oscilloscope.

B. N Atom Detection Cell. Photodissociation of N_2O and laser detection of atomic nitrogen were conducted in a quartz cell with Suprasil laser entry and exit windows which had a third window (quartz) perpendicular to the entry and exit windows for monitoring the fluorescence. Gas flow to the cell was from a 2.5 cm diameter quartz tube, through which either a slow flow of N_2O or the products of an N_2 microwave discharge, including atomic nitrogen, were carried to the laser interaction region. A diagram of the laser photodissociation and detection cell is shown in Figure 2. For the photolysis experiments, the N_2O would flow from a sidearm gas inlet directly to the laser interaction cell where photodissociation and TALIF detection would occur. The experimental conditions included a 5 sccm slow flow of pure nitrous oxide with no active discharge. For experiments requiring production of atomic nitrogen in a discharge, N_2 flowed through a sidearm gas inlet within an Opthos 2.45 GHz microwave discharge cavity before entering the laser interaction cell (shown as an option in Figure 2). The sidearm gas inlets were positioned so that N_2O could be added downstream of the discharge but before the laser probe region to test the collisional quenching effect of N_2O on the excited atomic N (3p) $^4S^\circ_{3/2}$ state. When the N_2O was added to the flowing afterglow region of the microwave discharge, the N_2 partial pressure was maintained at 2 Torr. With the TALIF signal

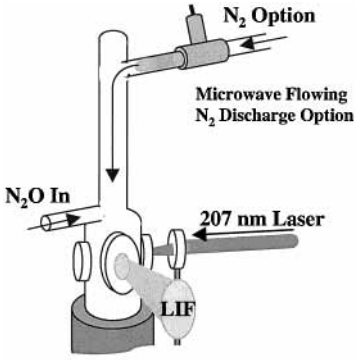

Figure 2. Diagram of the laser photodissociation and detection cell including the sidearm that provides option of N_2 flowing microwave discharge.

quenching effects of N_2 well established,[10] the quenching effect of the added N_2O was extracted from an analysis of the fluorescence decay lifetime. Gas flow and pressure in the microwave discharge system were governed by a mass flow controller/downstream throttle value combination which was controlled by an MKS-146 control unit. A diaphragm pump backed oil free molecular drag pump evacuated the discharge cell.

C. Fraction of Photolyzed N_2O in TALIF Region. In this work, quenching rates of the laser excited state of N atom photogragments have been quantified and attributed to collisions with ground state N_2O. This relies on the assumption that the number density of background N_2O greatly exceeds any other species generated during the photolysis of N_2O. A rough estimate of the number density of photofragments compared to the N_2O background gas supports this assumption. The estimated number density of excited-state nitrous oxide, $[N_2O]^*$, produced by 207 nm absorption can be used to gauge the number density of photofragments in the photolysis region since most of the excited N_2O states below 6 eV are pre-dissociative. The number density, $[N_2O]^*$, within the laser focal region can then be given as

$$[N_2O]^* \approx \frac{\mu}{Al}\frac{I_a}{I_o} \tag{3}$$

where I_a/I_o is the fraction of laser light absorbed within the focal region, μ is the number of incident photons, A is the cross sectional area of the beam focus, and l is the length of the focal region. If the Beer−Lambert law is assumed to be valid in the laser focal region, the laser light absorption may then be expressed as[8]

$$I_a/I_o = (1 - e^{-kpl}) \tag{4}$$

where k is the absorption coefficient of N_2O in $Torr^{-1}$ cm^{-1} and p is the N_2O pressure. With $k = 10^{-3}$ $Torr^{-1}$ cm^{-1} for 207 nm light,[11] $p < 1$ Torr, and $l < 1$ mm; therefore, $kpl \ll 1$ so that

$$[N_2O]^* \approx \frac{\mu kp}{A} \tag{5}$$

Thus, a nitrous oxide pressure of 0.5 Torr and a laser pulse energy of 0.2 mJ with a beam diameter of 200 μm results in $[N_2O]^* = 2 \times 10^{14} cm^{-3}$, which is approximately 1% of the $[N_2O]$ in the region. This small $[N_2O]^*/[N_2O]$ fraction indicates that the N_2, O, and NO photofragments, as well as any molecules produced in fast secondary reactions, are not likely to be major contributors to the N atom (3p) $^4S^o_{3/2}$ state quenching in this experiment.

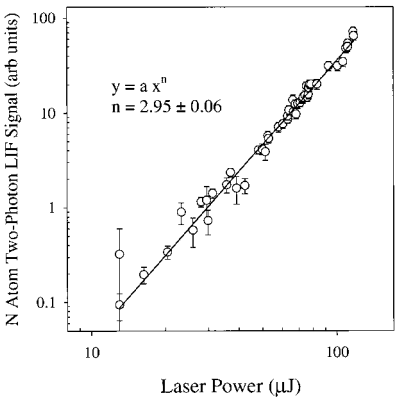

Figure 3. Laser pulse energy dependency plot of the two-photon LIF signal of the atomic nitrogen photofragment produced from photodissociation of N_2O.

Results and Discussion

A. Photodissociation Energy Analysis. The 207 nm laser power dependency of the TALIF signal was analyzed to experimentally determine whether the N_2O photodissociation was single- or multiphoton induced. These data provided the first experimental verification that this secondary photodissociation process of N_2O, producing the observed atomic nitrogen fragment, was indeed a single-photon event, as suggested in previous work.[9] The results of the analysis are shown in Figure 3 for a slow flow of N_2O with no discharge. Since the TALIF signal scales, within uncertainty, with the cube of the laser pulse energy, the absorption was determined to be a three-photon process, including a single-photon dissociation plus the two-photon detection. The laser power dependency of the two-photon LIF signal alone was calibrated with an N_2 discharge source, which confirmed that laser saturation effects were not a factor in the TALIF detection under the conditions of interest.

B. Collisional Quenching Results. Analysis of the fluorescence decay from the (3p) $^4S^o_{3/2}$ state of the N atom photofragment in the presence of photolyzed N_2O was done for a slow flow of N_2O at a cell pressure of 0.05 Torr to 0.8 Torr. The decay constant determined in the analysis is equal to $1/\tau_d$, which is defined as

$$\frac{1}{\tau_d} = \sum_i k_{qi}[M]_i + \frac{1}{\tau_r} \tag{6}$$

where τ_r is the radiative decay lifetime and the sum is over all the species present after the N_2O photolysis, with $[M]$ being the number density and k_q the quenching rate of each species. To determine the decay constant, $1/\tau_d$, from experimental data, we deconvolved the temporally resolved TALIF signal from the pulse laser temporal profile and photomultiplier temporal response function, both of which are described in section IIA. An example of the collisional quenching effect on the decay of the fluorescence signal is shown in Figure 4 for background N_2O pressures of 0.2 and 0.8 Torr of N_2O. The decay constant, $1/\tau_d$, is found from the deconvolved fluorescence signal to be 0.047 ns^{-1} for 0.2 Torr and 0.080 ns^{-1} for 0.8 Torr. Since the density of each of the collision partners in the photolysis interaction region is not known, an effective quenching rate,

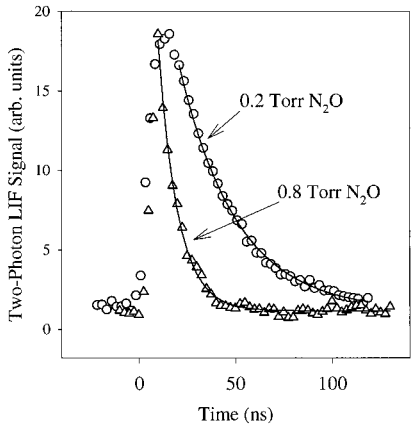

Figure 4. Temporally resolved experimental fluorescence signals at 0.2 Torr (circles) and 0.8 Torr (triangles) of N_2O demonstrate the reduction in excited-state lifetime with increased N_2O background pressure due to collisional quenching. Solid lines represent the fit of the signal decay.

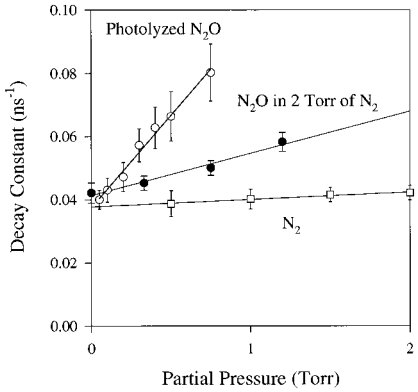

Figure 5. Stern−Volmer plot of atomic nitrogen (3p) $^4S^\circ_{3/2}$ state decay with quenching by photolyzed N_2O products, N_2O, and N_2.

k'_q, due to the collective quenching of all species is introduced as

$$k'_q[N_2O] = \sum_i k_{qi}[M]_i \tag{7}$$

where k'_q is coupled with the number density of nitrous oxide in the cell prior to photolysis. The results in Figure 5 show that the species in the N_2O photolysis region quench the N atom upper state very rapidly, with an effective quenching rate of $k'_q = (5.2 \pm 0.9) \times 10^7$ Torr^{-1} s^{-1} or $(1.6 \pm 0.3) \times 10^{-9}$ cm^3/s.

To isolate the quenching effects of N_2O as a collision partner with the N atom (3p) $^4S^\circ_{3/2}$ state, we introduced N_2O downstream of a 2 Torr of N_2 microwave discharge. On the basis of TALIF signal strengths, the discharge was found to produce 2 orders of magnitude more of atomic nitrogen than photodissociation of N_2O alone. The discharge source was far enough from the N_2O interaction region that the N atoms should be thermalized to ~300 K. The decay constant of the TALIF upper state in this case behaves as

$$\frac{1}{\tau_d} = k_{q(N_2O,300K)}[N_2O] + k_{q(N_2,300K)}[N_2] + \frac{1}{\tau_r} \tag{8}$$

The quenching rate, $k_{q(N_2,300K)}$, is found by varying only the partial pressure of nitrous oxide in the post-discharge mix. The result, determined from the plot in Figure 5, is that $k_{q(N_2,300K)} = (1.3 \pm 0.3) \times 10^7$ Torr^{-1} s^{-1} or $(4.2 \pm 1.0) \times 10^{-10}$cm^3/s. In previous work,[10] we determined the quenching of N atom (3p) $^4S^\circ_{3/2}$ by N_2 at 300 K to be $k_{q(N_2,300K)} = (2.1 \pm 0.3) \times 10^6$ Torr^{-1} s^{-1} or $(6.7 \pm 0.9) \times 10^{-11}$cm^3/s. These results are also shown in Figure 5 for comparison with the N_2O quench.

C. Discussion of TALIF Quenching by N_2O. Quenching of the N atom (3p) $^4S^\circ_{3/2}$ state by nitrous oxide at 300 K was found be 4.2×10^{-10}cm^3/s, which is a factor of 6 greater than the rate of quenching by molecular nitrogen. The measured rate, though, is still a factor of 4 smaller than the effective quenching rate measured in the photolysis experiments. The difference in the quench rates between the two experiments can be shown to be a direct result of excess kinetic energy imparted to the atomic nitrogen during photodissociation.

To deduce kinetic information for the recoiling N atom from the quenching data, it is necessary to determine the major collision partners of the N atom in the photolysis region. The molecules N_2 and NO are both present in the photolysis region as products of N_2O photodissociation, but their contribution to the N (3p) $^4S^\circ_{3/2}$ quenching was calculated to be negligible during the short lifetime of the TALIF signal. The density ratio of photolytically produced N_2 to N_2O was estimated to be 1% from the calculations in section IIC, and the [NO]-to-[N_2O] ratio can be estimated to be <0.02% when considering the branching ratio of the secondary photodissociation path. The corresponding [N_2] and [NO] densities were determined to be too small to substantially contribute to the observed quenching in the photolysis region, even when assuming gas kinetic reaction rates between the recoiling molecule and the excited N atom. Thus, kinetic information for the recoiling N atom may be derived from the effective quenching rate of N (3p) $^4S^\circ_{3/2}$ in the photolysis region by assuming the quenching is due only to collisions with N_2O.

The collisional quenching rate can be expressed as

$$k_q = \langle \sigma_q(v) v \rangle \tag{9}$$

where v is the mean relative speed of collision and $\sigma_q(v)$ is the quenching cross section in cm^2. Over a small spread of velocities, $\sigma_q(v)$ can be assumed to be constant, given as $\langle \sigma_q \rangle$, and can be determined by

$$\langle \sigma_q \rangle = \frac{k_q}{\langle v \rangle} \tag{10}$$

In the experiment where N_2O was added to the discharge afterglow, the excited N atoms and N_2O reacting in the afterglow were assumed to be in thermal equilibrium at $T = 300$ K. The mean relative speed between two colliding particles, each with a Maxwellian velocity distribution, can be found by[12]

$$\langle v \rangle = \sqrt{\frac{8kT}{\pi m_{1,2}}} \tag{11}$$

where $m_{1,2} = m_1 m_2/(m_1+m_2)$ is the reduced mass of the colliding particles. For the case of excited N atoms and N_2O colliding at 300 K, the mean relative speed is found to be $\langle v \rangle = 77\,300$ cm/s, and a quenching rate for N(3p) $^4S^\circ_{3/2}$ by N_2O of $k_{q(N_2O,300K)} = 4.2 \times 10^{-10}$ cm^3/s with equation 10 yields $\langle \sigma_{q(300K)} \rangle = (54 \pm 13) \times 10^{-16}$ cm^2.

Now, when the photolysis experiment is considered, the 4-fold increase in quenching of N atom photofragments by N_2O indicates a significant N atom recoil velocity. When the quenching rate measured in the photolysis experiment and the quenching cross section at 300 K are used, with the assumption that the cross section does not vary with mean relative speed,

the average N atom recoil velocity after photolysis is

$$\langle v\rangle = \frac{k'_q}{\langle\sigma_q\rangle} = \frac{1.6\times10^{-9}\ \mathrm{cm^3/s}}{54\times10^{-16}\ \mathrm{cm^2}} = 296\,000 \pm 87\,000\ \mathrm{cm/s} \tag{12}$$

The average kinetic energy of the atomic nitrogen photofragment, given by

$$\langle\epsilon_N\rangle = \frac{1}{2}m\langle v\rangle^2 \tag{13}$$

is then 0.6 ± 0.2 eV, or ~16 times the kinetic energy of atomic nitrogen at 300 K.

This value of $\langle\epsilon_N\rangle$ can be checked against the theoretically maximum N atom recoil energy, which is determined from the laser photolysis photon energy (5.99 eV for 207 nm) and the N−NO bond energy (4.93 eV[3]). The difference in the photon energy and bond energy of $\epsilon_{(N+NO)} = 1.06$ eV is the energy available for photofragment kinetic energy as well as internal excitation of the photofragments. The maximum possible N atom recoil kinetic energy would occur with no internal energy excitation of the NO fragment. By conservation of momentum, the N atom fragment would have a maximum kinetic energy of

$$\epsilon_{N(max)} = \frac{m_{NO}}{m_{NO}+m_N}\epsilon_{(N+NO)} = 0.72\ \mathrm{eV} \tag{14}$$

This shows that the average recoil kinetic energy of 0.6 eV found in the quenching analysis is within the upper kinetic energy limit of 0.72 eV for the atomic nitrogen photofragment from N_2O photodissociation with 207 nm radiation.

D. Doppler Broadening of N atom Absorption Line in Discharge. A direct method of determining the velocity of the N atom photofragments is to analyze the Doppler broadening of the two-photon absorption line. The experimental absorption line shape spectrum was first studied in the afterglow of the microwave discharge where the atomic nitrogen was, to a good approximation, in thermal equilibrium at 300 K. For the thermal equilibrium condition, a Maxwell−Boltzmann velocity distribution can be assumed for which a normalized two-photon absorption line shape is

$$g(\nu) = \frac{2\sqrt{\ln(2)}}{\sqrt{\pi}(2\Delta\nu_L^2+\Delta\nu_D^2+2\Delta\nu_N^2)^{1/2}}\times \exp\left(-\frac{4\ln(2)(2\nu-\nu_o)^2}{(2\Delta\nu_L^2+\Delta\nu_D^2+2\Delta\nu_N^2)}\right) \tag{15}$$

where $\Delta\nu_L$ is the fwhm frequency spread of the laser radiation, $\Delta\nu_N$ is the natural line width of the two-photon transition, which is usually comparatively small, and $\Delta\nu_D$ is the fwhm of the Doppler broadening of the line. The fwhm of the Doppler broadened line is given by the formula[8]

$$\Delta\nu_D = \frac{2\sqrt{2\ln(2)}}{c}\nu_o\sqrt{\frac{kT}{M}} \tag{16}$$

where ν_o is the peak absorption frequency, M is the atomic mass, k is the Boltzmann constant, T is the temperature of the absorbing species, and c is the speed of light.

The Doppler broadening of the thermalized N atoms at 300 K in the afterglow can be calculated from eq 16 to be 0.32 $\mathrm{cm^{-1}}$. Assigning this value to the Doppler width created the opportunity to experimentally determine the laser line width contribution to the broadening of the two-photon absorption line shape. Figure 6 shows the N atom absorption line shape spectrum in the afterglow, along with a least-squares fit of eq 15 to the data. With $\Delta\nu_D$ set to 0.32 $\mathrm{cm^{-1}}$ and $\Delta\nu_N$ negligible, the $\Delta\nu_L$, the laser line width at 207 nm, is 0.63 $\mathrm{cm^{-1}}$. Since this 207 nm laser line width was a system constant, a Gaussian laser line shape component with $\Delta\nu_L = 0.63$ $\mathrm{cm^{-1}}$ was used in the subsequent Doppler broadening analysis for the photolysis experiment.

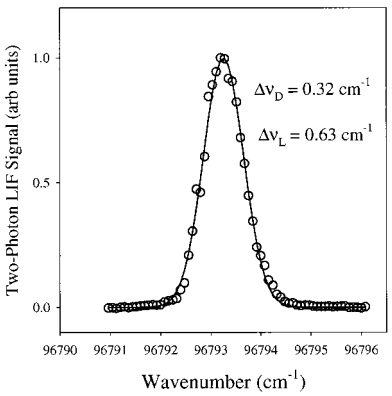

Figure 6. Two-photon absorption line shape spectrum data (circles) for thermalized atomic nitrogen at 300 K in the afterglow produced by a N_2 microwave discharge where $\Delta\nu_D$ was calculated from Doppler broadening theory and $\Delta\nu_L$ was determined from fit (solid line).

E. Doppler Broadening of N atom Photofragment Absorption Line. The TALIF quenching data presented in section IIIC suggests that atomic nitrogen produced by photodissociation of N_2O recoils with an average speed that greatly exceeds the average speed of thermalized N atoms at 300 K in the afterglow. This increase in average speed of the atomic nitrogen photofragments gives rise to an increased Doppler broadening of the two-photon absorption line shape. In contrast to the line shape analysis in section IIID for thermalized N atoms, the photodissociation process produces a recoil velocity distribution which is in general nonisotropic and non-Boltzmann.[13] Since we used a single linearly polarized laser as the dissociation and probe source, the velocity distribution of N atom photofragments is of the form[13]

$$W(v,\theta) = \frac{1}{4\pi}W(v)\left[1-\frac{\beta(v)}{2}P_2(\cos\theta)\right] \tag{17}$$

where θ is the angle between the laser propagation vector and the recoil direction, $W(v)$ is the normalized N atom speed distribution averaged over all angles, P_2 is the second Legendre polynomial where $P_2(x) = (^3/_2)x^2 - {}^1/_2$, and β is the anisotropy parameter, with limiting values of 2 and −1 representing fragment recoil parallel and perpendicular to the laser polarization, respectively.

The parameter v_k can be defined for convenience as the velocity component of a recoiling N atom in the direction of laser beam propagation, so that $\cos\theta = v_k/v$. The Doppler profile can then be determined as a function of v_k corresponding to the directional distribution in eq 17. The normalized Doppler profile, $g(v_k)$, for a single fragment recoil speed, v, is[14]

$$\begin{aligned} g(v_k) &= (2cv_o)^{-1}\left[1-\frac{1}{2}\beta(v)P_2(v_k/v)\right]; && \text{for } v_k \le v \\ g(v_k) &= 0; && \text{for } v_k > v \end{aligned} \tag{18}$$

where the latter condition gives a zero result since the velocity component, v_k, may not exceed the recoil speed, v. The Doppler

profile corresponding to the entire speed distribution of recoiling N atoms can now be determined by integrating eq 18 as

$$G(v_k) = \int_{|v_k|}^{\infty} \frac{W(v)}{2vv_o}\left[1 - \frac{\beta(v)}{2}P_2\left(\frac{v_k}{v}\right)\right] dv \qquad (19)$$

For the purpose of analyzing the two-photon absorption spectrum of the recoiling atomic nitrogen, the Doppler profile in eq 19 can be rewritten in terms of laser frequency, ν, using the Doppler relation $\nu = \nu_o(1 - v_k/c)$ so that

$$G(\nu) = \int_{c|\nu-\nu_o|/\nu_o}^{\infty} \frac{W(v)}{2vv_o}\left[1 - \frac{\beta}{2}P_2\left(\frac{(\nu-\nu_o)c}{v\nu_o}\right)\right] dv \qquad (20)$$

The velocity dependence of the anisotropy parameter, $\beta(v)$, was neglected in this analysis since the precision of this measurement did not allow for such a determination. Instead, an effective β was determined which represented the entire speed distribution. The convolution of the expression in eq 20 with the laser line shape and the parent molecule Doppler distribution produces a line shape that may be used to fit the experimental N atom absorption spectrum.

A unique determination of both the speed distribution, $W(v)$, and the anisotropy parameter, β, is generally not possible when analyzing only a single Doppler profile, such as when employing a single laser for dissociation and probing.[13] A determination of both $W(v)$ and β is achieved in this work by including the additional information on the average recoil velocity of the N atom fragments obtained through the quenching analysis in section IIIC. The process of fitting the absorption spectrum data included introducing various select functions of $W(v)$ to eq 20 and varying β to find the least-squares fit to the Doppler profile data. The $W(v)$ functions selected for fitting included speed distributions calculated from simple N atom kinetic energy distributions, $F(\epsilon_N)$. The velocity and kinetic energy of the atomic photofragment are related by $\epsilon_N = {}^1/_2\, mv^2$, with their respective normalized distributions related by

$$W(v(\epsilon_N)) = F(\epsilon_N)mv(\epsilon_N) \qquad (21)$$

Kinetic energy distributions of delta functions, Gaussian functions, and exponential increasing functions were introduced to the problem with the constraints that $\langle\epsilon_N\rangle = 0.6 \pm 0.2$ eV, as determined in the quenching analysis and that $F(\epsilon_N) = 0$ for $\epsilon_N > \epsilon_{N(max)} = 0.72$ eV, in accordance with the energy limitation of the two-photon absorption, as discussed in section IIIC.

The absorption line shape data in this experiment were best fit using an exponentially increasing atomic nitrogen kinetic energy distribution, which had a normalized form of

$$\begin{aligned} &F(\epsilon_N) = 1/b\, \exp[(\epsilon_N - \epsilon_{N(max)})/b]; && \text{for } \epsilon_N \le \epsilon_{N(max)} \\ &F(\epsilon_N) = 0; && \text{for } \epsilon_N > \epsilon_{N(max)} \end{aligned} \qquad (22)$$

where $1/b$ determines the exponential rise of the function. The mean kinetic energy of this distribution is

$$\langle\epsilon_N\rangle = \epsilon_{N(max)} - b\left[1 - \exp\left(\frac{-\epsilon_{N(max)}}{b}\right)\right] \qquad (23)$$

which can be approximated by $\langle\epsilon_N\rangle = \epsilon_{N(max)} - b$ since $\epsilon_{N(max)}$ is sufficiently large compared to b for this set of data. The constant b can then be given as $b = \epsilon_{N(max)} - \langle\epsilon_N\rangle$, which allows the atomic nitrogen kinetic energy distribution function to be

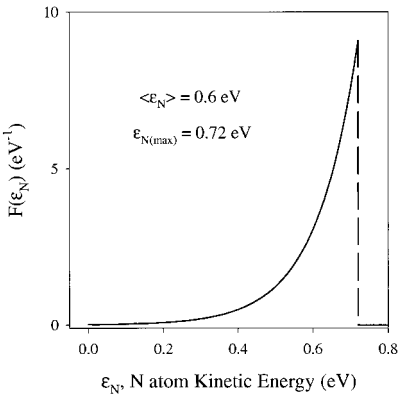

Figure 7. Normalized kinetic energy model distribution of atomic nitrogen fragments recoiling from N_2O photodissociation.

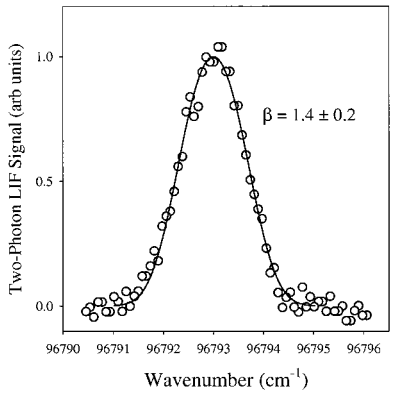

Figure 8. Two-photon absorption line shape spectrum data (circles) for atomic nitrogen photofragments produced by photodissociation of N_2O with 207 nm laser radiation. Solid line represents best fit with eq 20 using the $\langle\epsilon_N\rangle = 0.6$ eV energy distribution in Figure 7.

expressed in terms of the known mean kinetic energy and the maximum kinetic energy as

$$\begin{aligned} &F(\epsilon_N) = (\epsilon_{N(max)} - \langle\epsilon_N\rangle)^{-1} \times && \text{for } \epsilon_N \le \epsilon_{N(max)} \\ &\quad \exp[(\epsilon_N - \epsilon_{N(max)})/\epsilon_{N(max)} - \langle\epsilon_N\rangle]; \\ &F(\epsilon_N) = 0; && \text{for } \epsilon_N > \epsilon_{N(max)} \end{aligned} \qquad (24)$$

The normalized kinetic energy distribution corresponding to the energy constraints $\langle\epsilon_N\rangle = 0.6$ eV and $\epsilon_{N(max)} = 0.72$ eV is shown in Figure 7. The normalized speed distribution corresponding to this kinetic energy distribution is

$$\begin{aligned} &W(v) = 2v(v^2_{(max)} - \langle v\rangle^2)^{-1} \times && \text{for } v \le v_{(max)} \\ &\quad \exp[(v^2 - v^2_{(max)})/(v^2_{(max)} - \langle v\rangle^2)]; \\ &W(v) = 0; && \text{for } v \le v_{(max)} \end{aligned} \qquad (25)$$

The expression in eq 25 is the N atom photofragment speed distribution that was used, along with eq 20 and convolved with eq 15, to determine the anisotropy parameter β by least-squares fit to the measured line shape data. For the line shape function in eq 15, we set $\Delta\nu_L = 0.63$ cm^{-1} and assumed $\Delta\nu_N$ to be negligible, as found in section IIID, and the fwhm of the Doppler broadening due to the parent N_2O speed at 300 K from eq 16 to be $\Delta\nu_D = 0.18$ cm^{-1}.

The result of the fitting process is shown in Figure 8, in which the data was best fit using an N atom distribution with $\langle\epsilon_N\rangle = 0.6$ eV and a β value of 1.4 ± 0.2. To determine the uncertainty in β across the range of $\langle\epsilon_N\rangle = 0.6 \pm 0.2$ eV, we also fit the data with N atom distributions corresponding to the upper and

lower limits of uncertainty for $\langle\epsilon_N\rangle$. The resulting best fits were with $\beta = 1.9 \pm 0.2$ and $\beta = 0.4 \pm 0.2$ for the upper and lower limits of $\langle\epsilon_N\rangle$, respectively. Since values of $\beta > 2$ are beyond the physical limits of $-1\ \beta < 2$, the result can be interpreted that β in this experiment is within the range of $0.2-2$. An anisotropy parameter value of less than 2 suggests that N atom recoil is not exclusively parallel to the laser polarization. The assumption of photodissociation from a bent N_2O state is consistent with this reduced value of β.

F. N and NO Photofragment Kinetic Energy Distribution. In section IIIC, the total kinetic energy distributed among the N and NO fragments after absorption of two 207 nm photons was calculated to be $\epsilon_{(N + NO)} = 1.06$ eV. TALIF data has indicated that the atomic nitrogen fragments recoil from the 207 nm photodissociation of N_2O with a distribution that has a mean N atom kinetic energy of

$$\langle\epsilon_N\rangle_{trans} = 0.6 \pm 0.2 \text{ eV} \quad (26)$$

The partitioning of kinetic energy into the translational and internal energy of the NO fragment can therefore be determined by conservation of energy and momentum. By conservation of momentum, the mean translational energy of the NO fragment is found to be

$$\langle\epsilon_{NO}\rangle_{trans} = \frac{m_N}{m_{NO}}\langle\epsilon_N\rangle_{trans} = 0.3 \pm 0.1 \text{ eV} \quad (27)$$

which corresponds to a mean speed of $140\,000 \pm 40\,000$ cm/s. The remaining energy must reside as internal energy within the NO photofragment with a mean value of

$$\langle\epsilon_{NO}\rangle_{int} = \epsilon_{(N + NO)} - \langle\epsilon_N\rangle_{trans} - \langle\epsilon_{NO}\rangle_{trans} = 0.2 \pm 0.1 \text{ eV} \quad (28)$$

Since the energy required to excite the $v = 1$ state of NO from the ground vibrational state is 0.23 eV,[15] there is some possibility of vibrational excitation, but the internal energy of NO is most probably rotational in nature. The rotational excitation of the NO photofragment is not unexpected since the N_2O photodissociative processes from 207 nm absorption all involve N_2O excited states that have C_s, or bent, symmetry as is shown in Figure 1.

Conclusion

Photodissociation of nitrous oxide with subsequent TALIF detection of atomic nitrogen, both using 207 nm laser radiation, was accomplished in a low-pressure N_2O cell, where the ground state $N(^4S)$ and $NO(X^2\Pi)$ fragments were secondary products of this photodissociative process. Analysis of the N atom TALIF signal as a function of laser power provided experimental verification that the secondary photodissociation process of N_2O producing the observed atomic nitrogen fragment was a single-photon process. The N atom (3p) $^4S^o_{3/2}$ state, excited by two-photon absorption, was determined to be quenched by N_2O in the photolysis region at a rate of $(1.6 \pm 0.3) \times 10^{-9}$cm^3/s. A separate measurement of N atom (3p) $^4S^o_{3/2}$ state quenching by isolated N_2O in the flowing afterglow of a microwave discharge, where the atomic nitrogen was assumed to be thermalized at 300 K, produced a lower quenching rate of $k_{q(N_2O)} = (4.2 \pm 1.0) \times {}^{-10}$cm^3/s. The difference in the quenching rates was attributed to a much higher mean speed of the recoiling atomic nitrogen photofragments compared to that of the thermalized atomic nitrogen. Analysis of the quenching data resulted in the assignment of the mean kinetic energy of the N atom photofragments as 0.6 ± 0.2 eV, with quenching almost entirely from collisions with background N_2O. According to energy and momentum conservation for the photodissociation event, the maximum recoil kinetic energy of the atomic nitrogen was 0.72 eV.

The Doppler broadening of the two-photon absorption spectrum of the recoiling atomic nitrogen was also examined. A model kinetic energy distribution of the N atom photofragments was generated which met the constraints of mean and maximum kinetic energy values determined in the quenching analysis. An exponentially increasing model energy distribution produced good fits of the N atom two-photon absorption line data. Effective anisotropy parameters from the analysis ranged from $\beta = 0.2$ to 2 over the average energy range of $\langle\epsilon_N\rangle = 0.6 \pm 0.2$ eV.

Assignments were also made for the translational and internal energy of the $NO(X^2\Pi)$ photofragment based on the mean kinetic energy of the recoiling atomic nitrogen. The mean NO translational kinetic energy was found to be 0.3 ± 0.1 eV. The mean internal energy of the NO molecule was found to be 0.2 ± 0.1 eV, indicative of mostly rotational excitation within the NO.

References and Notes

(1) Tserepi, A. D.; Dunlop, J. R.; Preppernau, B. L.; Miller, T. A. *J. Appl. Phys.* **1992**, *72*, 2638−2643.
(2) Tserepi, A. D. Laser Diagnostics for Bulk and Near-Surface Detection of Atomic Hydrogen and Oxygen in Plasma Environments. PhD thesis, The Ohio State University, Columbus, OH, 1994.
(3) Hopper, D. G. *J. Chem. Phys.* **1984**, *80* (9), 4290−4316.
(4) Suzuki, T.; Katayanagi, H.; Mo, Y.; Tonokura, K. *Chem. Phys. Lett.* **1996**, *256*, 90−95.
(5) Hanisco, T. F.; Kummel, A. C. *J. Phys. Chem.* **1993**, *97*, 7242−7246.
(6) Felder, P.; Haas, B. M.; Huber, J. R. *Chem. Phys. Lett.* **1991**, *186*, 177−182.
(7) Shafer, N.; Tonokura, K.; Matsumi, Y.; Tasaki, S. *J. Chem. Phys.* **1991**, *95*, 6218−6223.
(8) Okabe, H. *Photochemistry of Small Molecules*; Wiley: New York, 1978.
(9) Bengtsson, G. J.; Larsson, J.; Svanberg, S.; Wang, D. D. *Phys. Rev. A* **1992**, *45*, 2712−2715.
(10) Adams, S. F.; Miller, T. A. *Chem. Phys. Lett.* **1998**, *295*, 305−311.
(11) Zelikoff, M.; Watanabe, K.; Inn, E. C. *J. Chem. Phys.* **1953**, *21*, 1643.
(12) Mitchner, M.; Kruger, C. H. *Partially Ionized Gases*; Wiley: New York, 1973.
(13) Dubs, M.; Bruhlmann, U.; Huber, J. R. *J. Chem. Phys.* **1986**, *84*, 3106−3119.
(14) Zare, R. N.; Herschbach, D. R. *Proc. IEEE* **1963**, *51*, 173.
(15) Huber, K.-P.; Herzberg, G. *Constants of Diatomic Molecules*; Van Nostrand Reinhold: New York, 1979.